Available online at www.sciencedirect.com
SCIENCE DIRECT
Tectonophysics 420 (2006) 357–369
TECTONOPHYSICS
www.elsevier.com/locate/tecto

Coulomb stress triggering of earthquakes along the Atalanti Fault, central Greece: Two April 1894 M6+ events and stress change patterns

A. Ganas [a,*], E. Sokos [a,1], A. Agalos [a], G. Leontakianakos [a], S. Pavlides [b]

[a] Geodynamics Institute, National Observatory of Athens, Lofos Nymfon, 118 10 Athens, Greece
[b] Department of Geology, Aristotle University of Thessaloniki, 541 24 Thessaloniki, Greece

Received 17 April 2005; received in revised form 5 February 2006; accepted 18 March 2006

Abstract

Two M6+ events occurred 15–20 km apart in central Greece on April 20 and April 27, 1894. We identify the April 27, 1894 rupture (2nd in the sequence) with the Atalanti segment of the Atalanti Fault Zone because of unequivocal surface rupturing evidence reported by Skouphos [Skouphos, T., 1894. Die swei grossen Erdbeben in Lokris am 8/20 und 15/27 April 1894. Zeitschrift Ges. Erdkunde zu Berlin, vol. 24, pp. 409–474]. Coulomb stress transfer analysis and macroseismic evidence suggest that the April 20, 1894 event (1st in the sequence) may be associated with the Martinon segment of the same fault zone. Our stress modelling suggests that this segment may have ruptured in an $M=6.4$ event producing a 15-km long rupture which transferred 1.14 bar in the epicentral area of the April 27th, 1894 event, thus triggering the second $M=6.6$ earthquake along the Atalanti segment and producing a 19-km long rupture. We also examined three alternative fault sources for the first event; however, all these produce smaller stress stresses for triggering the second event. The proposed slip model for the second earthquake is capable of producing coastal subsidence of the order of centimetres to decimetres, which fits the geological data. The 1894 earthquake sequence was followed by a difference in the timing of subsequent $M>5$ events in each of the "relaxed" areas (stress shadows; a negative change in Coulomb failure stress > -0.6 bar), which terminated between 22–37 years (north) and 80 years (south).

Keywords: Stress transfer; Seismicity; Active faulting; Atalanti; Deformation; Central Greece

1. Introduction

The Atalanti Fault is a large, active normal fault in central Greece with an average strike of N290°E and a dip to the northeast (Fig. 1; Lemeille, 1977; Rondoyianni-Tsiambaou, 1984; Ambraseys and Jackson, 1990; Ganas et al., 1998; Pantosti et al., 2001, 2004; Pavlides et al., 2004). The fault is a Late Pliocene–Quaternary structure and accommodates crustal extension across the Gulf of Evia rift (Fig. 1). The fault starts a few kilometres to the northwest of the town of Atalanti and terminates near the town of Larymna, about 34 km to the southeast (Fig. 2; Ganas et al., 1998). The fault ruptured during the 1894 earthquake sequence when two main shocks occurred 15–20 km apart with a time difference of one week (April 20 and 27, 1894; Skouphos, 1894; Ambraseys and Jackson, 1990). The earthquakes killed more than 250 people, injured several hundred and shattered thousands of houses

* Corresponding author. Tel.: +30 210 3490186; fax: +30 210 3490180.
E-mail address: aganas@gein.noa.gr (A. Ganas).
[1] Now with Department of Geology, University of Patras, Patras, GR.

0040-1951/$ - see front matter © 2006 Elsevier B.V. All rights reserved.
doi:10.1016/j.tecto.2006.03.028

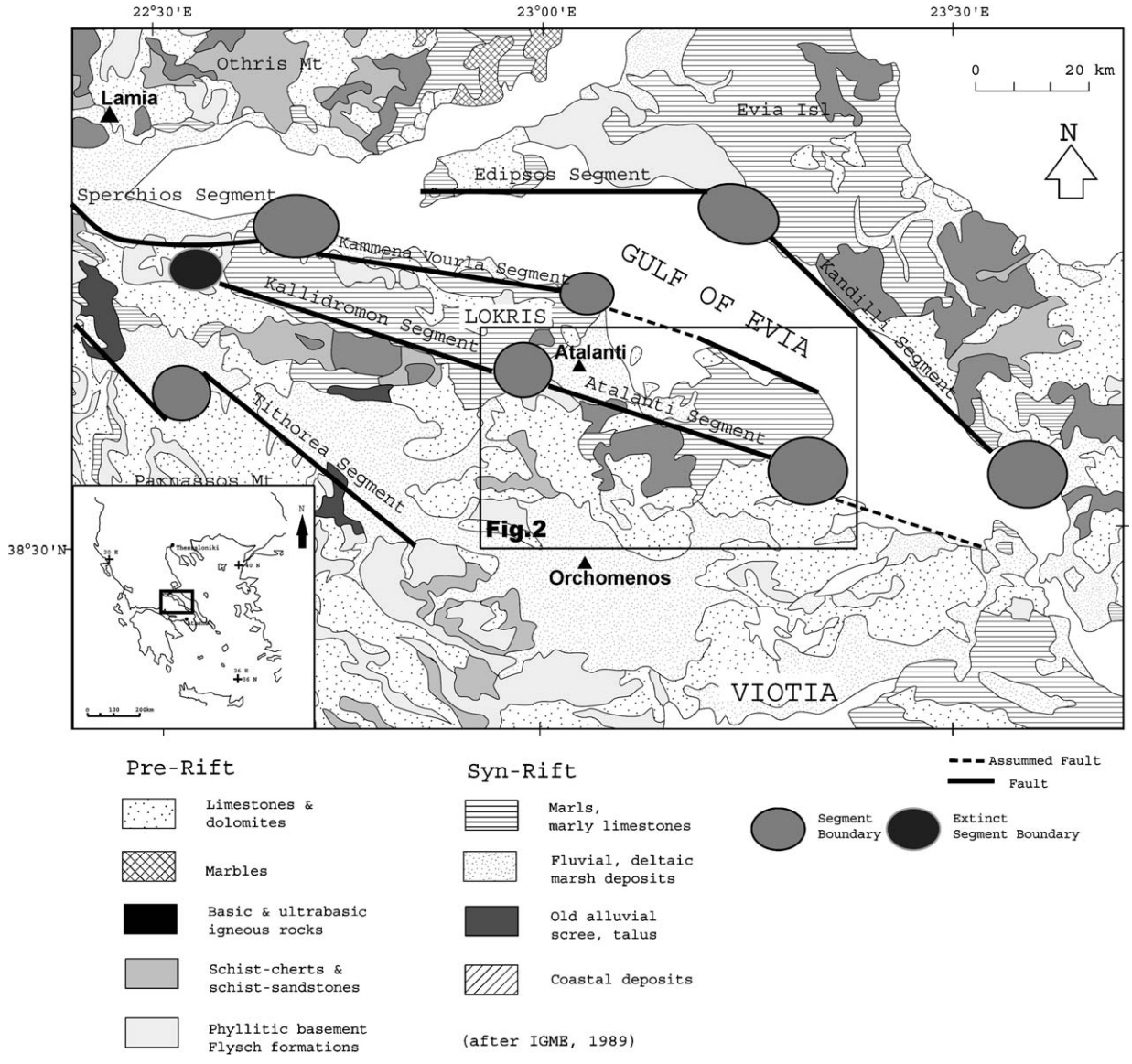

Fig. 1. Geological map of the Lokris area (central Greece), modified after IGME (1989). Simplified fault lines are after Ganas and Papoulia (2000). Rectangular box at centre shows extent of Fig. 2. Note that the Atalanti Fault segment is decomposed into two (2) earthquake segments in Fig. 2. Inset box shows regional setting.

thus creating a legendary event in Modern Greek history (Mitsopoulos, 1895).

From the work of Skouphos (1894), it is known that the 27 April 1894 earthquake ruptured the fault plane from the coastal plain of Kyparissi up to the town of Atalanti (Fig. 3). An open question (Ganas et al., 1998) is whether this rupture extended all the way to Larymna towards the southeast or whether it terminated a few kilometers to the south, near the village of Proskinas (P in Fig. 2). In the latter case, the Atalanti Fault may have ruptured in both events (20 and 27 April), each event filling a fault segment. The second segment would be the portion of the fault plane between Atalanti town and Proskinas village, a distance of about 19 km. The initial rupture would have been on the Martinon segment of the same fault (Fig. 2). However, if the 27 April 1894 surface breaks were extending as far as Larymna, then the earlier event of 20 April 1894 may be associated with another normal fault in the region, such as a coastal normal fault offshore Malesina Peninsula or a normal fault to the southeast (Pantosti et al., 2001; see Fig. 5 for possible sources and Table 1 for their characteristics).

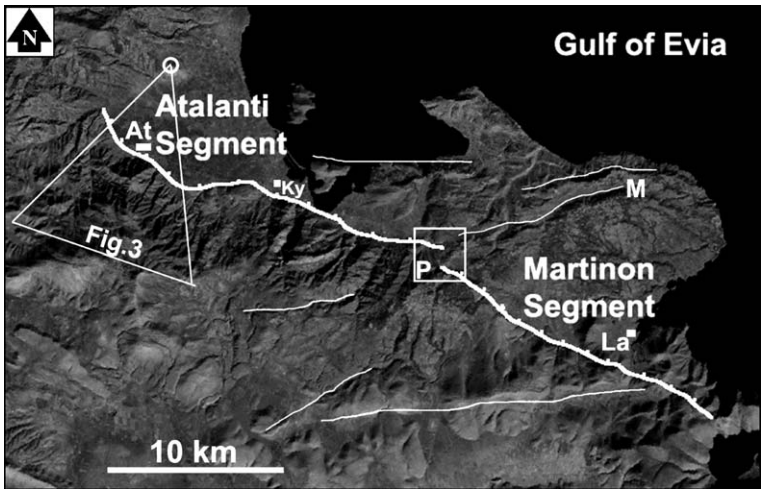

Fig. 2. Landsat satellite image showing earthquake segment position along the Atalanti Fault Zone. The two segments are represented as white lines with ticks on the downthrown side. Thin white lines represent other normal faults, which are oriented favorably to the current stress field. La symbol denotes the town of Larymna, At the town of Atalanti, M the Malesina Fault, P the Proskynas area and Ky the village of Kyparissi, respectively.

Normal fault segment interaction within the Aegean region has been documented in the 1981 Gulf of Alkyonides sequence (Hubert et al., 1996), the 1904 Kresna earthquakes (Ganas et al., 2005) and has been proposed for the 1978 Thessaloniki earthquake (triggered by the 1932 Ierissos event; Nalbant et al., 1998) and the south Thessaly earthquake sequence between 1954 and 1957 (Papadimitriou and Karakostas, 2003). All these cases involved spatial and temporal clustering of $M>6$ earthquakes along normal faults accommodating N–S extension of the Aegean crust as it was the 1894 earthquake sequence which occurred inside the

Fig. 3. Field photograph of the northwestern Atalanti segment. White arrows point to the location of the fault trace along the mountain front. Curved white arrow indicates “wine-glass” valley. White triangles indicate faceted spurs. View to the southwest.

Table 1
The slip models of source faults shown in Fig. 5

#	Name	Epicentre	Length (km)	Strike	Dip (°)	Rake	U_d (m)	U_s (m)	Mw
1	Martinon	38.583–23.233	15	300	55	− 70	0.69	0.25	6.4
2	Malesina	38.633–23.241	12	245	55	− 122	0.39	0.24	6.2
3	Coastal	38.700–23.250	15	290	55	− 80	0.72	0.12	6.4
4	Anthedon	38.550–23.417	15	300	55	− 70	0.69	0.25	6.4
5	Atalanti	23.083–38.667	19	290	55	− 80	1.05	0.18	6.6

Features include: source event epicentre coordinates (latitude–longitude), fault length, strike (clockwise from north), dip, rake, average dip slip per event, average strike slip per event, earthquake magnitude. Fault width is 12 km in all cases. The Mw is calculated after Hanks and Kanamori (1979). The geological data are after Ambraseys and Jackson (1990) and Ganas et al. (1998).

northern Gulf of Evia juvenile rift (Fig. 1; Roberts and Jackson, 1991; Ganas and Papoulia, 2000; Roberts and Ganas, 2000). This paper investigates first the possibility that the event of 27 April 1894 on the northwestern segment of the Atalanti Fault was triggered by the earthquake of 20 April 1894 on the southeastern segment of the same fault due to static stress transfer (e.g., Reasenberg and Simpson, 1992; Stein et al., 1992). Then also examines other triggering scenarios for the 1894 events by calculating the static stress transferred to the Atalanti segment as a result of co-seismic slip on a number of source faults identified in Fig. 5 (Table 1). Our findings suggest that the most favorable stress transfer scenario occurs if the April 20, 1894 earthquake ruptured the Martinon segment.

2. The macroseismic field of the April 1894 earthquakes

In April 1894, two devastating earthquakes occurred in the region of Lokris (along the southern coast of the Gulf of Evia), within a week (Skouphos, 1894;

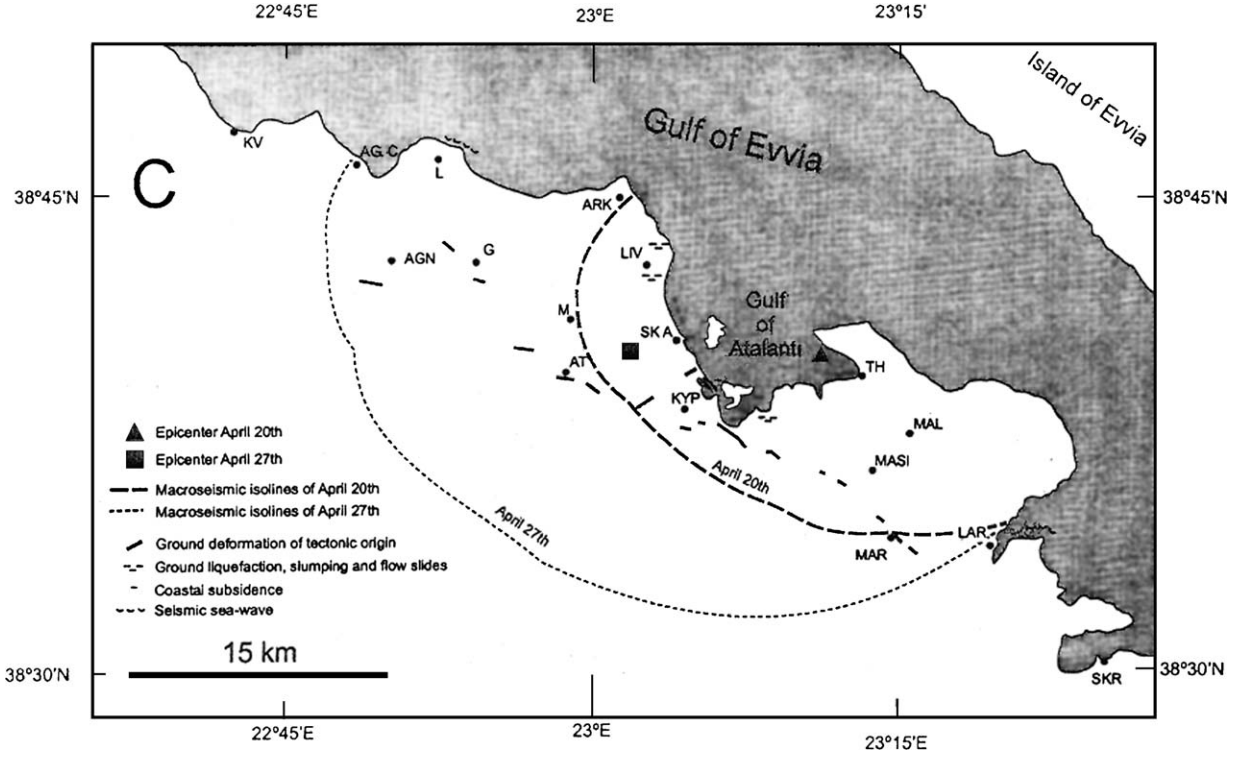

Fig. 4. Map of the greater Atalanti area showing the macroseismic effects of the 1894 earthquake sequence (after Cundy et al., 2000). Names of towns as follows: KV=Kammena Vourla, AGC=Agios Constantinos, L=Loggos, AGN=Agnadi, G=Goulemi, AT=Atalanti, M=Megaplatanos, ARK=Arkitsa, LIV=Livanates, SKA=Skala, KYP=Kyparissi, TH=Theologos, MAL=Malesina, MASI=Mazi, MAR=Martinon, LAR=Larymna, SKR=Skroponeri (after Cundy et al., 2000 and Ambraseys and Jackson, 1990).

Mitsopoulos, 1895). Severe loss of life and property were reported along the coastal region (Fig. 4), as well as surface rupturing and ground-shaking phenomena. The severely damaged region was aligned in a general NW–SE direction with minor damage in the neighbouring areas of Viotia and the island of Evia (Fig. 4). Sea inundation was reported along the whole of the coastline in the greater Kyparissi area (Fig. 4). Skouphos (1894, pp. 410–421) describes earthquake-related ground phenomena, such as 100-m long ground-cracks with infinitesimal throw (or no throw at all), resulting from the first event (20 April 1894) and shows that they were restricted to the Malesina Peninsula (Fig. 2). In contrast, damage associated with the second, stronger event (at 9:17 p.m. of 27 April 1894) extended for more than 30 km to the northwest, and major ruptures exhibiting both opening and throw were noted. Up to 2 m of throw were recorded where the rupture crossed alluvium, with only 30 cm of throw recorded in limestone bedrock. Although several short ground-cracks (less than 100–150 m) and landslides were mentioned by Skouphos in the region to the north and northwest of the town of Atalanti, no descriptions of throw values were included. Following re-examination of the geological and historical evidence, Ganas et al. (1998) suggested that the continuous rupture produced by the second earthquake did not cross the Atalanti–Kallidromon segment boundary (Fig. 1).

Skouphos describes surface breaks along the foothills of the Chlomon Mountain (Fig. 3), as well as inside of, and in the vicinity of the town of Atalanti that was totally devastated. Mitsopoulos (1895) in his field report apparently refers to the same breaks as extending from Atalanti to the Almyra region (the coastal area near Kyparissi in Fig. 2) and "in parallel sets to the main ground rupture". The observations of these authors indicate that the rupture mostly followed the prerift–synrift contact, i.e., the main fault plane along the mountain front (Fig. 3). The repetition of many earthquakes in this area has formed a characteristic footwall geomorphology with triangular facets and "wine-glass" valleys (Fig. 3). Further south, in the Kyparissi area (Fig. 4), Skouphos (1894, p. 446) reported two surface breaks with a 25–45-cm aperture, enclosing a "semi-elliptical" region (about 2 km long and 800 m wide).

Albini and Pantosti (2004) analysed coeval records on the effects of the 1894 in order to assess macroseismic intensities according to the European Macroseismic Scale. An intensity equal or higher than 8 has been estimated at 70 different places in both Lokris and Evia, respectively. To image the earthquake sources and derive the main seismic parameters, they processed the macroseismic intensity data by using the Boxer method proposed by Gasperini et al. (1999). On the basis of this approach, they obtained M 6.4 and 6.5 for the 20 and 27 April earthquakes, respectively, the latter being substantially smaller than the estimates proposed in previous works. Results obtained from the processing of macroseismic data have been tested and compared to geological data, as well. Their preferred interpretation is that the 20 and 27 April 1894 earthquakes ruptured together the whole Atalanti Fault. They suggest that the structural complexity of the Atalanti Fault appears to have controlled the rupture propagation. They identified a change in strike of the fault trace along with its intersection with the Malesina Fault, near Proskinas (see Fig. 2), which is interpreted as a geometric barrier that is the boundary between the two individual earthquake sources. The 20 April earthquake would have ruptured between Proskinas and Skroponeri Mountains, southeast of the village of Larimna (Fig. 4), whereas the 27 April earthquake ruptured between Proskinas and the northwest Chlomon Fault Zone, north of the town of Atalanti.

3. Earthquake segmentation model

The April 27, 1894 earthquake ruptured the prerift/synrift contact in the region of Atalanti–Martinon (Skouphos, 1894; Fig. 2). The prerift rocks are: (a) hard, resistant carbonates occurring mainly near Kyparissi and Larymna; (b) an ophiolitic complex of ultrabasic rocks near the villages of Kyparissi and Proskinas; and (c) a volcano-sedimentary unit near Atalanti which lies at the base of the sub-Pelagonian zone of the Hellenides (Figs. 1 and 3). The synrift rocks are Pliocene and Pleistocene sediments. The Pliocene comprises sands, clays, yellow marls and well-sorted pebbles, formed in a fluvio-lacustrine environment. The Pleistocene sediments are alluvial fan deposits, talus cones and scree, fluvial conglomerates and breccias. The sedimentary basin is developed more to the northwest (Ganas et al., 1998) and fault throws diminish gradually to the southeast. This asymmetry in fault growth may reflect a complexity in earthquake occurrence along this fault.

Due to the uncertainty in defining the 1894 rupture pattern and in order to calculate the static stress transfer, we make two important assumptions: (a) the Atalanti normal fault is formed of two segments which join in the area near the village of Proskinas (Fig. 2) and (b) both segments were close to failure during April 1894. The first assumption is supported by the geological data of Poulimenos and Doutsos (1996), Ganas et al. (1998), Pantosti et al. (2001) and Pavlides et al. (2004). The field data show a right step along strike of the Atalanti

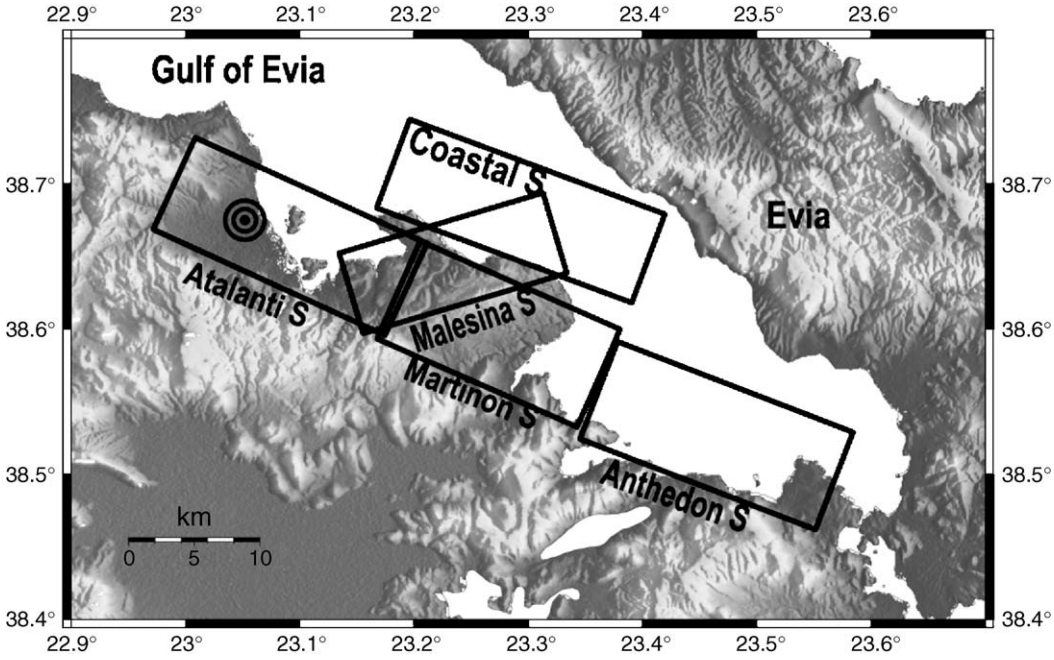

Fig. 5. Relief map showing location of source fault segments (Martinon, Anthedon, Coastal and Malesina) and the receiver fault (Atalanti) within the greater Atalanti region, central Greece. Boxes represent approximate surface projections of rectangular dislocations. All NW–SE oriented faults have normal geometry and dip to the northeast. Source Malesina is oriented NE–SW and downthrows to the northwest. Concentric circles indicate epicentre of the 27 April 1894 event according to Ambraseys and Jackson (1990).

Fault Zone near the village of Proskinas (Fig. 2). The step is visible in satellite images and may be regarded as (a) soft linkage structure and/or (b) the location of the segment boundary. Geomorphological evidence also supports the existence of a boundary because drainage patterns change across the village of Proskinas (Ganas et al., 1998). The second assumption is reasonable to accept because of the large recurrence intervals of earthquakes along the Atalanti Fault (Pantosti et al., 2004); the last large pre-1894 event most probably occurring between AD 770 and 1160 (Pantosti et al., 2004). The alternate possibility case that the 20 April 1894 event occurred on a separate fault than the Atalanti Fault is treated separately by considering nearby faults as potential sources for that event (Fig. 5). The detailed modeling is presented below.

4. Coulomb stress modeling

Large earthquakes on normal fault planes can trigger subsequent earthquakes at short distances from the epicentre by transferring static or dynamic stresses (e.g., Harris et al., 1995; Caskey and Wesnousky, 1997; Nostro et al., 1997; Harris and Simpson, 1998; Gomberg et al., 2001). We computed static stress changes due to simple, planar slip along several source faults using the DLC code by R. Simpson (USGS). Modeling parameters are summarized in Table 2. We compute the Coulomb stress change in an elastic half-space (Okada, 1992) by assuming a shear modulus of 3.0×10^{10} Pa, Poisson's ratio 0.25 and apparent coefficient of friction $\mu'=0.4$. Value 0.4 was adopted as is closer to friction values for major faults (Harris and Simpson, 1998). The fault slip models are based on field data by Ambraseys and Jackson (1990) with updates from Ganas and Buck (1998), Ganas et al. (1998) and Pantosti et al. (2001). All source faults are normal slip planes. No active strike-slip faults near Atalanti have been found in recent seismicity studies (e.g., Hatzfeld et al., 1999; Kiratzi, 2002). The 20 April 1894 sources share similar fault length (L) and width (W) values (15 and 12 km), respectively, except for the Malesina Fault, which is shorter by about 20%. All

Table 2
Input parameters used for stress transfer modeling

Poisson ratio	0.25
Shear modulus	μ=300,000 bar
Map projection	UTM zone 34
Depth of ΔCFF calculation	10 km
Grid size	1 km
Friction coefficient (μ')	0.4
Target planes	290/55/− 80

sources were modeled as inclined, rectangular dislocations ignoring local fault complexities. The Ambraseys and Jackson (1990) coordinates for the 1894 earthquake epicentres were used on the basis of their macroseismic and field reports. We calculated the change in the Coulomb Failure Function (CFF) on target failure planes (e.g., Reasenberg and Simpson, 1992),

$$\Delta\mathrm{CFF} = \Delta\tau + \mu'\Delta\sigma_n \quad (1)$$

where $\Delta\tau$ is the co-seismic change in shear stress on the receiver fault and in the direction of fault slip, $\Delta\sigma_n$ is the change in normal stress (with tension positive) and μ' is the effective coefficient of friction,

$$\mu' = \mu(1 - \Delta P/\Delta\sigma_n) \quad (2)$$

where μ is the static coefficient of friction and ΔP is the pore pressure change within the fault. ΔCFF is the Coulomb stress change between the initial, Coulomb stress and the final stress. ΔCFF was sampled on a horizontal section at 10-km depth on a 100×100-km grid surrounding the source event epicentre, with 1-km grid spacing (Fig. 6). First, we used the program ELFGRID to calculate a stress tensor grid at 10-km depth. Then, we applied the program STROP, which uses that tensor to calculate the tractions at that depth on planes of specified orientation. STROP outputs a ΔCFF file that does the calculation in Eq. (1) above on the planes of interest for the friction value specified. The spatial distribution of the Coulomb stress has a lobate pattern, which is often approximately symmetric with respect to fault rupture (Fig. 6). We interpret a positive value of ΔCFF to mean that a fault plane occurring within this lobe has been brought closer to failure; when ΔCFF is negative, the fault is brought further from failure (i.e., relaxed). A value 0.4 for the effective coefficient of friction was adopted that is typical of friction values used in stress transfer studies (Harris and Simpson, 1998).

To evaluate the triggering capability of the assumed source faults, we calculated the amount of Coulomb stress which was transferred to the epicentral area of the 27 April 1894 event (23.083E, 38.667N) for the following scenarios: (a) source fault to be the Martinon segment (Fig. 6a), (b) source fault to be the Malesina segment suggested by Pantosti et al. (2001) (Fig. 6b), (c) source fault to be the coastal fault, offshore Theologos Bay (Ganas and Buck, 1998), and (d) source fault to be the offshore fault to the southeast of Larymna (Anthedon segment) where fresh fault planes have been mapped by Rondoyianni-Tsiambaou (1984). We obtained the following stress levels: for case (a) 1.14 bar (114 kPa), case (b) 0.52 bar, case (c) 0.45 bar and case (d) 0.09 bar. We note that the first three cases result in substantial difference in the amount of Coulomb stress transferred with the first case differing by a factor of 2 from case (b) and case (c). Other studies in central Greece (e.g., Hubert et al., 1996) and elsewhere (e.g., Parsons et al., 2000) inferred that 1–2 bar of transferred stress were capable of triggering large earthquakes on neighbouring segments as in our case (a). However, Harris et al. (1995) indicated that ΔCFF levels >0.1 bar are associated with earthquake triggering on neighbouring faults. Therefore, we cannot exclude cases (b) and (c), as possible scenarios and perhaps even case (d) because no lower triggering threshold has yet been established (e.g., Ziv and Rubin, 2000). Thus, our Coulomb stress results need to be combined with other information in order to constrain the most probable triggering scenario. It seems that the macroseismic effects of the 20 April 1894 event described by Skouphos (1894) and re-examined by Ambraseys and Jackson (1990, Fig. 4) and Albini and Pantosti (2004) point to case (a).

5. Discussion–conclusions

5.1. 1894 rupture scenario

Our static stress transfer calculations and the macroseismic effects of the 20 April 1894 event favor successive rupturing of earthquake segments along the Atalanti Fault in the 1894 pair of events. We suggest rupture of the Martinon segment (case 6a) during the 20 April 1894 event although the most proximal potential source to the 27 April 1894 epicentral area is the Malesina normal fault (Fig. 5). This is because of the following reasons: (a) there is geological evidence that the Malesina Fault is inactive today (Ganas et al., 1998) as: (i) it does not show fresh fault planes, (ii) there are no Quaternary-age deposits on its hangingwall, (iii) the fault is both cut by the younger Atalanti Fault and the coastal fault (Fig. 2) and (iv) the drainage is directed N–S and not NE–SW as it should be if the fault was controlling local drainage; (b) the strike of the Malesina Fault (N245°E) with respect to the regional stress field (N14°E; Roberts and Ganas, 2000) is not optimal in order to produce the maximum Coulomb stress change along Atalanti-type faults. To conform to the regional extension direction, the rake of the Malesina slip vector has to trend up to − 122° (i.e., this results in a significant dextral oblique-slip component). However, this kinematic requirement is not supported by geological

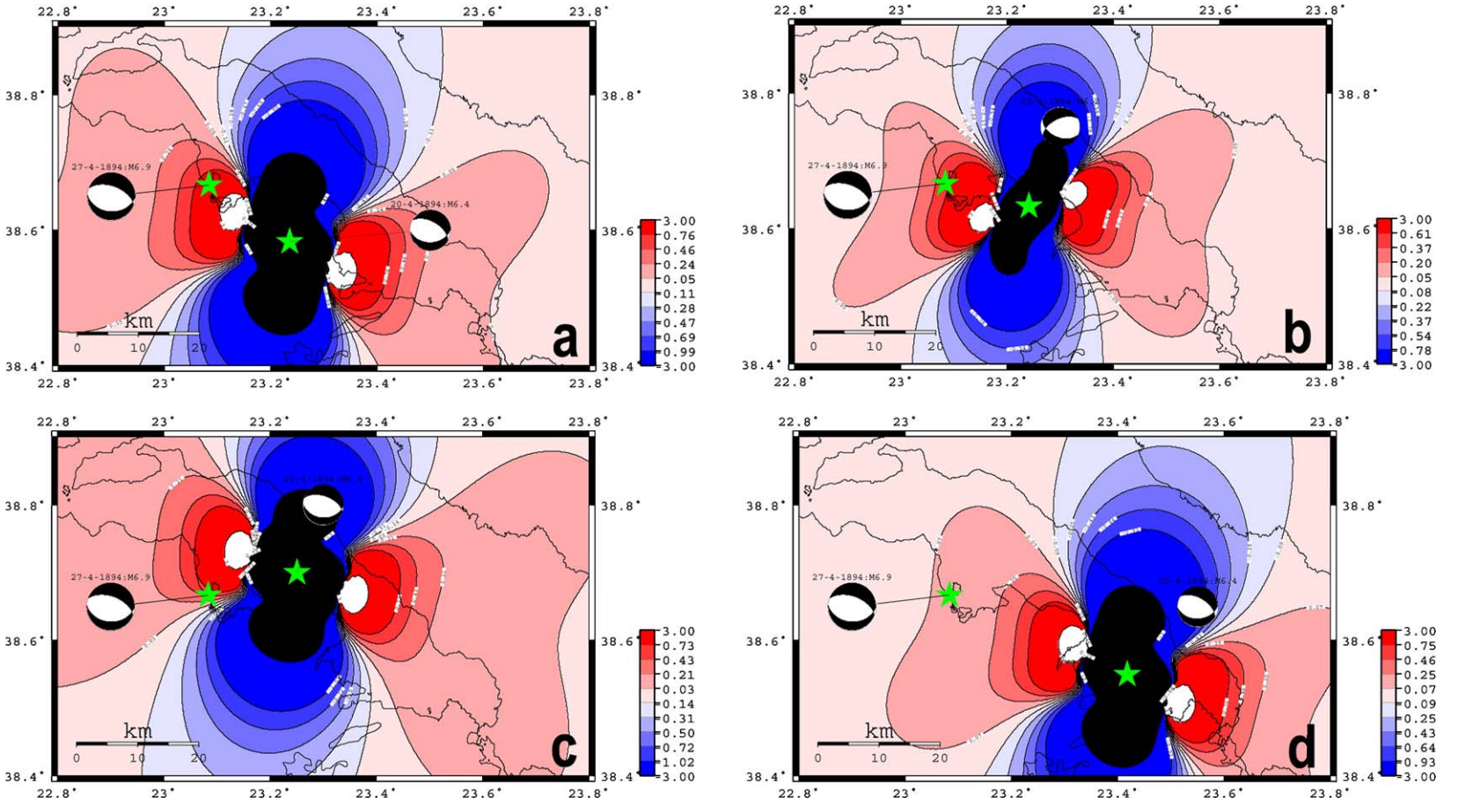

Fig. 6. Coulomb stress changes at 10-km depth associated with the 20-4-1894 earthquake in central Greece. Colour palette of stress values is histogram-equalised in the range − 3 to + 3 bar. White colour indicates area where transferred stress >3 bar and black colour the area where stress reduction was > −3 bar. (a) Map produced by rupturing the Martinon segment. Green stars show the 1894 earthquake epicentres. (b) Map produced by rupturing the Malesina segment proposed by Pantosti et al. (2001). Source fault has oblique right-lateral slip with strike/dip/rake of 245°/55°/− 122° (see text for discussion). (c) Coastal fault segment case. (d) Anthedon segment case. Source segments are shown in Fig. 4. Coulomb stress calculated for Atalanti-type normal faults (i.e. strike N290°E, dip 55°NE) in all cases. Blue areas indicate unloading, red areas indicate loading, respectively. Effective coefficient of friction is 0.4 in all cases. Slip models are shown in Table 1. Beachballs represent low hemisphere, equal area projections of fault plane solutions. Colour scale in bar (1 bar=100 kPa).

observations on slip vector orientations in the area around Malesina (Rondoyianni-Tsiambaou, 1984; Ganas et al., 1998; Roberts and Ganas, 2000). Third, in our modeling, the fault was assigned a length of 12 km, i.e., its length is 20% shorter than the other source faults (Table 1) because (a) it is seen on satellite images to terminate against the Atalanti segment (western end; Fig. 2) and (b) it disappears towards the sea (eastern end; Fig. 2) where relief is controlled by the NW–SE coastal normal fault. So, assuming this fault is active, its surface rupture length should not produce an earthquake >Ms 6.2 according to the empirical relationship of Wells and Coppersmith (1994), which is a smaller magnitude suggested by the macroseismic data (Ambraseys and Jackson, 1990; Albini and Pantosti, 2004). The conclusion from our stress transfer modeling is supported by a recent re-appraisal of the macroseismic data (Albini and Pantosti, 2004).

Our results also indicate that the April 1894 earthquake sequence advanced rupture times of normal faults in areas to the northwest and southeast of the Atalanti Fault (Fig. 7). We can estimate this time advance using recent seismological data for this area of Greece. Assuming a stress drop of 9–27 bar for central Greece earthquakes (Tselentis and Zahradnik, 2000; Benetatos et al., 2002) and recurrence intervals for the Gulf of Evia segments between 660 and 1120 years (Pantosti et al., 2001), then the remote loading rate ranges between 0.04 bar/year and 0.008 bar/year. For ΔCFF values of 1 bar that were computed at a distance of approximately 10 km from the fault tips (Fig. 7), the amount of transferred stress implies loading times of 25–125 years. On the other hand, faults to the south and to the north have had their rupture times delayed due to a reduction of their stress levels.

5.2. The magnitude of the second earthquake and post-1894 seismicity

Several moderate shocks ($M<6.0$) occurred in the years after 1894 in the positively stressed area inside the Gulf of Evia rift (Fig. 7), within a 30-km radius of the 27 April 1894 epicentre. Our earthquake catalogue (Table 3) is complete for the period 1901–1999 for $M>5$. In addition, for the period May 1894–1901, no events $M>6$ are reported by Galanopoulos (1982) for this region. However, no data for events $M<6.0$ exist

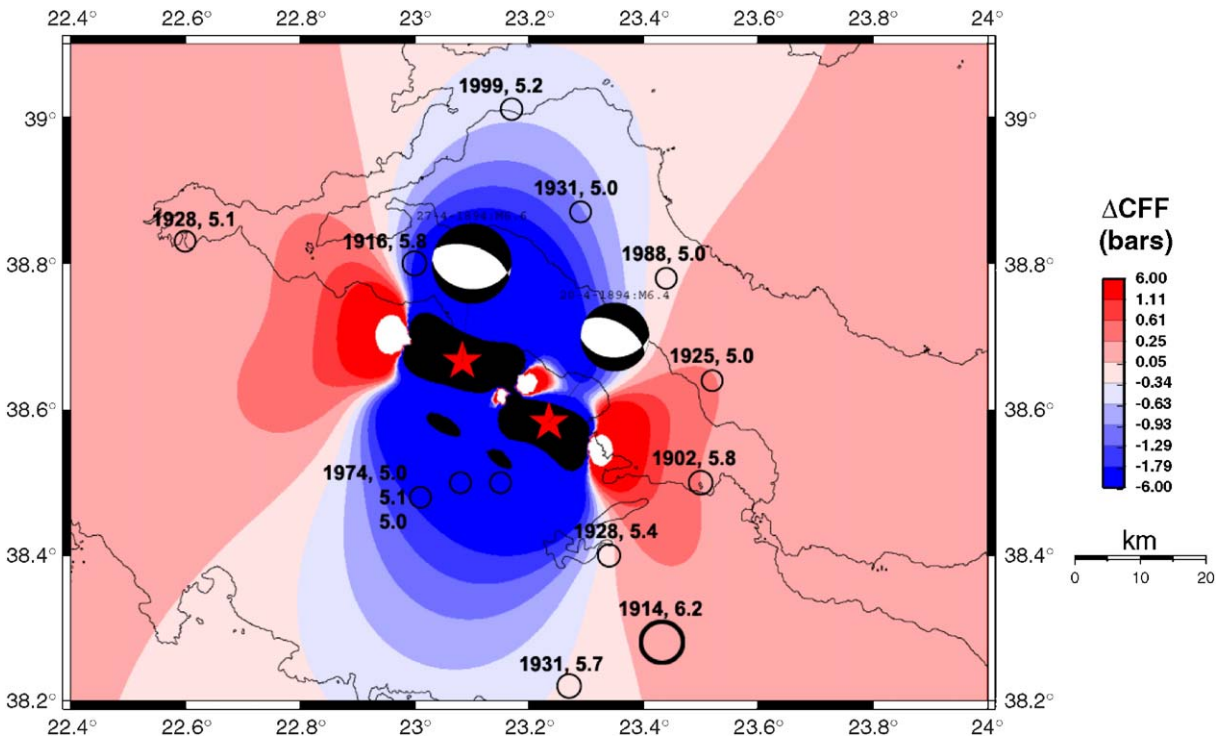

Fig. 7. Co-seismic static stress changes produced by the combination of two M6+ earthquakes in the Atalanti area, central Greece. Coulomb stress calculated for the two earthquakes along Atalanti-type faults at 8-km depth. Colour palette is histogram-equalised with red colour indicating positive stress change, blue the opposite. The effective coefficient of friction is 0.4. Circles indicate epicentres of earthquakes greater than 5.0 Ms for the period 1901–1999.

Table 3
Catalogue of shallow events in the Gulf of Evia region during the 20th century

Year	Month	Day	Hour	Minute	Second	Latitude	Longitude	Ms	Dist
1902	April	11	18	35	0	38.50	23.50	5.8	45
1914	October	17	06	22	32	38.31	23.44	6.2	52
1916	September	27	15	02	13.0	38.80	23.00	5.8	22
1925	April	12	19	27	0.9	38.64	23.52	5.0	45
1928	January	22	00	18	26.0	38.83	22.60	5.1	43
1928	April	22	19	59	29.4	38.40	23.34	5.4	37
1931	January	4	00	00	52.5	38.22	23.27	5.7	48
1931	September	11	16	23	22.7	38.87	23.29	5.0	39
1974	November	14	13	22	34.7	38.50	23.08	5.0	13
1974	November	14	14	26	46.6	38.48	23.01	5.1	13
1974	November	14	15	29	46.8	38.50	23.15	5.0	17
1988	July	12	02	26	53.3	38.78	23.44	5.0	43
1999	February	7	22	28	37.7	39.01	23.17	5.2	48

Column Ms reports surface magnitude and column Dist reports distance of event to the April 27, 1894 epicentral area. All events have occurred within a circle of 55-km radius from Atalanti (38.60N, 23.00E). Events are plotted in Fig. 7. Data are from Comninakis and Papazachos (1986) and NOA Bulletins. The errors involved in the magnitudes are in the interval of ± 0.2 for the instrumental period (1911–1999).

for the period 1894–1901. In other words, there is a possibility that events in the magnitude range 5–6 may have occurred in this area other than the 1894 aftershocks. Despite this data gap, we suggest that the lack of strong ($M>6$) events for at least 110 years may be due to a combination of factors such as (in order of descending importance): (1) the long recurrence intervals of earthquakes along the segments of Gulf of Evia rift as suggested by their slow slip rates (Ganas et al., 1998; Pantosti et al., 2001; 0.1–0.5 mm/year); (2) the low geodetic strains (40–65% less) in comparison to the Gulf of Corinth rift (Davies et al., 1997). A third reason is that perhaps the magnitude of the 27 April 1894 event was less than is widely believed (Ms 6.9, Ambraseys and Jackson, 1990; M 7.0, Papazachos and Papazachou, 2003, p. 238). We suggest a Mw 6.6 on the basis of the 1894 segmentation model (Fig. 5 and Table 1). Using the Wells and Coppersmith (1994) relationship $\log D = (0.69\pm0.08)\mathrm{Mw} - (4.80\pm0.57)$, we obtain that a 6.6 magnitude reduces co-seismic slip by about 38% relative to a 6.9 event and would transfer less Coulomb stress to nearby faults. In addition, the 6.6 magnitude fits better the Wells and Coppersmith (1994) global relationship between 19-km rupture length and earthquake magnitude ($\mathrm{Mw} = 4.86 + 1.32\log[\mathrm{SRL}]$). The same magnitude results after applying the Pavlides and Caputo relationship for the Aegean region ($M = 0.90\log[\mathrm{SRL}] + 5.48$; Pavlides and Caputo, 2004). We also note that an M 6.5 has been proposed for the 27 April 1894 event on the basis of the macroseismic data (Albini and Pantosti, 2004). Finally, the 6.6 magnitude event would be expected to cause surface subsidence on the order of centimeters to decimeters in the coastal plain near Kyparissi (Fig. 2). This figure is compatible with the findings of Cundy et al. (2000) who studied the coastal subsidence pattern and favour a multi-segmented Atalanti Fault.

In terms of identifying seismogenic potential for nearby faults, we note that the E–W striking, Kamena Vourla–Arkitsa normal fault segment (Kamena Vourla segment in Fig. 1) has received Coulomb stress loading during both the 20 April 1894 and 27 April 1894 events, which together added more than 1 bar to its stress level. This fault is active (Jackson and McKenzie, 1999; Roberts and Ganas, 2000; Pavlides et al., 2004) and it may be close to failure because crustal deformation has also been detected by microgravity measurements (Lagios et al., 1988). We suggest that the seismic hazard posed by this segment is greater in comparison to that posed by other faults in the area (Fig. 1) because of our static stress calculations. This fault is seismically quiescent and current microseismic activity was detected to the south of it, inside the Renginion basin (Hatzfeld et al., 1999). We also point to a possibly triggered event, in 1914 near Thiva (Fig. 7). This event is located approximately 50 km to the southeast of Atalanti, in a region where stress levels along E–W striking faults have been increased by approximately 0.2 bar due to the two mainshocks of the 1894 sequence. If the 1914 fault was close to failure, then the Atalanti events may have further promoted this destructive earthquake.

5.3. Duration of the stress shadow effect

The 20th century seismicity map of the Evia region (for $M>5$) shows a small number of events occurring inside “stress shadows”. These are areas of the crust that

have been subjected to a decrease in stress levels greater than 0.6 bar by the events in 1894. They form a lobate pattern in map view on either side of the Atalanti Fault extending to distances of about 30 km (the blue areas of Fig. 7). We chose to set the threshold at − 0.6 bar because it is possible that during the post-1894 period earthquakes with $M<5$ have occurred at distances longer than 30 km on either side from the Atalanti Fault (still inside the outer negative lobe) and were not recorded by NOA. In the area to the south of the Atalanti Fault, the 1974 earthquake sequence near Orchomenos (see Fig. 1 for location) occurred in the middle of a "stress shadow" at a distance of 15 km from the 1894 mainshocks. This area had been subjected to a stress decrease >1.8 bar after 27 April 1894 (first southern blue lobe in Fig. 7). In the area to the north of Atalanti, there were two events above 5.0 Ms, in 1916 and 1931, within a distance of 15–30 km. The 1931 sequence has been well located by NOA recordings (NOA, 1943) as occurring in the northern Evia region, which is located within the northern blue lobe. This area is about 30 km to the north of the 1894 mainshocks and stress levels had been suppressed more than 0.9 bar. The 1916 event is most probably associated with rupturing of the Edipsos segment (Fig. 1; Ganas and Papoulia, 2000). However, the uncertainty associated with the 1916 epicentre does not permit its certain assignment within either the "loaded" or the "shadow" area (Fig. 7). In the first case, it can be argued that the 1916 event was triggered by the 1894 sequence because it is located inside the area with a Coulomb stress increase of >0.2 bar. In the second case where this earthquake has occurred a few kilometres to the east, then its location is within the first northern blue lobe (stress reduction >1.8 bar) and its distance from the 1894 mainshocks about 15 km. This analysis suggests that stress levels in the vicinity of the Atalanti Fault have recovered within a period of 22–37 years in the region to the north and 80 years in the region to the south, respectively.

This difference in stress recovery time demonstrates an asymmetrical temporal effect that may be related to (a) a difference in tectonic loading between the two areas on either side of the Gulf of Evia rift, (b) erosion of the northern shadow by stress transfer to Evia from earthquakes in the Aegean Sea (e.g., Nalbant et al., 1998; Papadimitriou and Sykes, 2001) or (c) prolongation of the stress shadow effect in the southern region due to post-1894 seismicity inside the Gulf of Corinth rift, which is located 50 km to the south (Fig. 1). The active faults of the eastern Corinth Rift strike approximately ENE–WSW (Roberts and Jackson, 1991; Roberts and Ganas, 2000; Kiratzi and Louvari, 2003) and Coulomb stress patterns following large normal-slip earthquakes should resemble those in Fig. 6, i.e., positive lobes to develop along the E–W direction and negative lobes to develop along the north–south direction. This configuration resembles the "negative feedback" mechanism of Cowie (1998) between faults. Although we have not investigated the evolution of seismicity and associated stress changes in the Gulf of Corinth, we note that hypothesis c is of particular interest because it implies that neighbouring rift systems spaced 50 km across strike can also interact the same way as individual fault segments within the same rift. Therefore, the duration of the stress shadow effect inside juvenile rift systems seems to be primarily a function of the slip rate of the active fault array and the across-strike spacing of rift systems.

Acknowledgements

Funding was partially provided by the Earthquake Protection and Planning Organisation of Greece and by the General Secretariat for Research and Technology. We thank Bob Simpson and one anonymous referee for constructive comments and Hans Thybo for editorial assistance. We also thank George Stavrakakis, Evangelos Lagios, Gerassimos Papadopoulos, Gerald Roberts, Ruth Harris and Vassilis Karastathis for comments. We are indebted to our students D. Keramydas, S. Sboras and S. Valkaniotis for their help during field works and literature search of the 1894 earthquakes. Some figures were prepared using the GMT software. The satellite image in Fig. 2 was provided by NASA free of charge. The Relief image in Fig. 4 originated from the SRTM 90 m global dataset.

References

Albini, P., Pantosti, D., 2004. The 20 and 27 April 1894 (Locris, central Greece) earthquake sources through coeval records on macroseismic effects. Bulletin of the Seismological Society of America 94 (4), 1305–1326.

Ambraseys, N.N., Jackson, J.A., 1990. Seismicity and associated strain of central Greece between 1890 and 1988. Geophysical Journal International 101, 663–708.

Benetatos, C., Roumelioti, Z., Kiratzi, A., Melis, N., 2002. Source parameters of the M 6.5 Skyros Island (North Aegean Sea) earthquake of July 26, 2001. Annals of Geophysics 45 (3–4), 513–526.

Caskey, S.J., Wesnousky, S.G., 1997. Static stress changes and earthquake triggering during the 1954 Fairview peak and Dixie valley earthquakes, central Nevada. Bulletin of the Seismological Society of America 87 (3), 521–527.

Comninakis, P.E., Papazachos, B.C., 1986. A catalogue of earthquakes in Greece and the surrounding area for the period 1901–1985. Univ. Thessaloniki. Geophysical Lab. Publication. 1, 167 pages.

Cowie, P.A., 1998. A healing-reloading feedback control on the growth rate of seismogenic faults. Journal of Structural Geology 20, 1075–1087.

Cundy, A.B., Kortekaas, S., Dewez, T., Stewart, I.S, Collins, P.E.F, Croudace, I.W, Maroukian, H., Papanastassiou, D., Gaki-Papanastassiou, P., Pavlopoulos, K., Dawson, A., 2000. Coastal wetlands as recorders of earthquake subsidence in the Aegean: a case study of the 1894 Gulf of Atalanti earthquakes, central Greece. Marine Geology 170 (1–2), 3–26.

Davies, R., England, P., Parsons, B., Billiris, H., Paradissis, D., Veis, G., 1997. Geodetic strain of Greece in the interval 1892–1992. Journal of Geophysical Research-Solid Earth 102 (B11), 24571–24588.

Galanopoulos, A., 1982. The earthquake potential of Greece. Annales Géologiques des Pays Helléniques 32, 647–724.

Ganas, A., Roberts, G., Memou, P., 1998. Segment boundaries, the 1894 ruptures and strain patterns along the Atalanti Fault, central Greece. Journal of Geodynamics 26, 461–486.

Ganas, A., Buck, V.A., 1998. A model for tectonic subsidence of the Allai archaeological site, Lokris, central Greece. Proceedings of the 8th International Congress of the Geological Society of Greece, pp. 181–187.

Ganas, A., Papoulia, I., 2000. High-resolution, digital mapping of the seismic hazard within the Gulf of Evia Rift, central Greece using normal fault segments as line sources. Natural Hazards 22 (3), 203–223.

Ganas, A., Shanov, S., Drakatos, G., Dobrev, N., Sboras, S., Tsimi, C., Frangov, G., Pavlides, S., 2005. Active fault segmentation in southwest Bulgaria and Coulomb stress triggering of the 1904 earthquake sequence. Journal of Geodynamics 40 (2–3), 316–333.

Gasperini, P., Bernardini, F., Valensise, G., Boschi, E., 1999. Defining seismogenic sources from historical earthquake felt reports. Bulletin of the Seismological Society of America 89, 94–110.

Gomberg, J., Reasenberg, P.A., Bodin, P., Harris, R.A., 2001. Earthquake triggering by seismic waves following the Landers and Hector mine earthquakes. Nature 411, 462–466.

Harris, R.A., Simpson, R.W., Reseanberg, P.A., 1995. Influence of static stress changes on earthquake locations in southern California. Nature 375, 221–224.

Harris, R.A., Simpson, R.W., 1998. Suppression of large earthquakes by stress shadows: a comparison of Coulomb and rate-and-state failure. Journal of Geophysical Research 103, 24439–24451.

Hanks, T.C., Kanamori, H., 1979. A moment magnitude scale. Journal of Geophysical Research 84, 2348–2350.

Hatzfeld, D., Ziazia, M., Kementzetzidou, D., Hatzidimitriou, P., Panagiotopoulos, D., Makropoulos, K., Papadimitriou, P., Deschamps, A., 1999. Microseismicity and focal mechanisms at the western termination of the North Anatolian Fault and their implications for continental tectonics. Geophysical Journal International 137 (3), 891–908.

Hubert, A., King, G., Armijo, R., Meyer, B., Papanastasiou, D., 1996. Fault re-activation, stress interaction and rupture propagation of the 1981 Corinth earthquake sequence. Earth and Planetary Science Letters 142, 573–585.

IGME (Institute of Mineral and Geological Exploration), 1989. Seismotectonic map of Greece. Scale 1:500000, Athens.

Jackson, J., McKenzie, D., 1999. A hectare of fresh striations on the Arkitsa fault, central Greece. Journal of Structural Geology 21 (1), 1–6.

Kiratzi, A.A., 2002. Stress tensor inversions along the westernmost North Anatolian Fault Zone and its continuation into the North Aegean Sea. Geophysical Journal International 151 (2), 360–376.

Kiratzi, A., Louvari, E., 2003. Focal mechanisms of shallow earthquakes in the Aegean Sea and the surrounding lands determined by waveform modeling: a new database. Journal of Geodynamics 36, 251–274.

Lagios, E., Drakopoulos, J., Hipkin, R.G., Gizeli, C., 1988. Microgravimetry in Greece: applications to earthquake and volcano-eruption prediction. Tectonophysics 152, 197–207.

Lemeille, F., 1977. Études néotectoniques en Grèce centrale nord-orientale (Eubée centrale, Attique, Béotie, Locride) et dans les sporades du nord (île de Skiros). Universite Paris, vol. XI. 173 pp. (in French).

Mitsopoulos, K., 1895. The Lokris Mega-Earthquake. Government publication, Athens (in Greek), 40 pp.

Nalbant, S.S., Hubert, A., King, G.C.P., 1998. Stress coupling between earthquakes in northwest Turkey and the North Aegean Sea. Journal of Geophysical Research 103, 24469–24486.

NOA, 1943. Annales de L'Observatoire National d'Athenes, Tome III (Geodynamique).

Nostro, C., Cocco, M., Belardinelli, M.E., 1997. Static stress changes in extensional regimes: an application to southern Apennines (Italy). Bulletin of the Seismological Society of America 87 (1), 234–248.

Okada, Y., 1992. Internal deformation due to shear and tensile faults in a half-space. Bulletin of the Seismological Society of America 82, 1018–1040.

Pantosti, D., De Martini, P.M., Papanastassiou, M., Palyvos, D., Lemeille, N., Stavrakakis, F., 2001. A reappraisal of the 1894 Atalanti earthquake surface ruptures, central Greece. Bulletin of the Seismological Society of America 91, 760–780.

Pantosti, D., De Martini, P.M., Papanastassiou, D., Lemeille, F., Palyvos, N., Stavrakakis, G., 2004. Paleoseismological trenching across the Atalanti Fault (central Greece): evidence for the ancestors of the 1894 earthquake during the middle ages and roman times. Bulletin of the Seismological Society of America 94 (2), 531–549.

Papadimitriou, E.E., Sykes, L.R., 2001. Evolution of the stress field in the northern Aegean Sea (Greece). Geophysical Journal International 146, 747–759.

Papadimitriou, E.E., Karakostas, V.G., 2003. Episodic occurrence of strong ($Mw \geq 6.2$) earthquakes in Thessalia area (central Greece). Earth and Planetary Science Letters 215, 395–409.

Papazachos, B.C., Papazachou, C.B., 2003. Earthquakes of Greece. Ziti, Thessaloniki, 286 pp. (in Greek).

Parsons, T., Toda, S., Stein, R.S., Barka, A., Dieterich, J.H., 2000. Heightened odds of large earthquakes near Istanbul: an interaction-based probability calculation. Science 288, 661–665.

Pavlides, S.B., Caputo, R., 2004. Magnitude versus faults' surface parameters: quantitative relationships from the Aegean region. Tectonophysics 380, 159–188.

Pavlides, S.B., Valkaniotis, S., Ganas, A., Keramydas, D., Sboras, S., 2004. The Atalanti active fault: re-evaluation using new geological data. Bulletin of the Geological Society of Greece 36, 1560–1567.

Poulimenos, G., Doutsos, T., 1996. Barriers on seismogenic faults in central Greece. Journal of Geodynamics 22, 119–135.

Reasenberg, P.A., Simpson, R.W., 1992. Response of regional seismicity to the static stress change produced by the Loma Prieta earthquake. Science 255, 1687–1690.

Roberts, S., Jackson, J., 1991. Active normal faulting in central Greece: an overview. Special Publication-Geological Society of London 148, 125–142.

Roberts, G.P., Ganas, A., 2000. Fault-slip directions in central and southern Greece measured from striated and corrugated fault planes: comparison with focal mechanism and geodetic data. Journal of Geophysical Research 105, 23443–23462.

Rondoyianni-Tsiambaou, Th., 1984. Etude néotectonique des rivages occidentaux du canal d'Atalanti (Grèce Centrale). Thèse 3me cycle. Univ. Paris-Sud, 190 pp.

Skouphos, T., 1894. Die swei grossen Erdbeben in Lokris am 8/20 und 15/27 April 1894. Zeitschrift der Gesellschaft für Erdkunde zu Berlin 24, 409–474.

Stein, R.S., King, G.C.P., Lin, J., 1992. Change in failure stress on the southern San Andreas Fault System caused by the 1992 magnitude=7.4 Landers earthquake. Science 258, 1328–1332.

Tselentis, G.A., Zahradnik, J., 2000. The Athens earthquake of 7 September 1999. Bulletin of the Seismological Society of America 90 (5), 1143–1160.

Wells, D.L., Coppersmith, K.J., 1994. New empirical relationships among magnitude, rupture length, rupture width, rupture area, and surface displacement. Bulletin of the Seismological Society of America 84, 974–1002.

Ziv, A., Rubin, A.M., 2000. Static stress transfer and earthquake triggering: no lower threshold in sight? Journal of Geophysical Research 105 (B6), 13631–13642.